Mixed excitonic nature in water-oxidized BiVO$_4$ surfaces with defects

Rachel Steinitz-Eliyahu [1], Daniel Hernangómez-Pérez [1], Franziska S. Hegner [2], Pavle Nikačević [2], Núria López,[2] and Sivan Refaely-Abramson [1,*]

[1]*Department of Molecular Chemistry and Materials Science, Weizmann Institute of Science, Rehovot 7610001, Israel*

[2]*Institut Català d'Investigació Química (ICIQ), The Barcelona Institute of Science and Technology (BIST), Avenida Països Catalans, 16, 43007 Tarragona, Spain*

BiVO$_4$ is a promising photocatalyst for efficient water oxidation, with surface reactivity determined by the structure of active catalytic sites. Surface oxidation in the presence of oxygen vacancies induces electron localization, suggesting an atomistic route to improve the charge transfer efficiency within the catalytic cycle. In this paper, we study the effect of oxygen vacancies on the electronic and optical properties at BiVO$_4$ surfaces upon water oxidation. We use density functional theory and many-body perturbation theory to explore the change in the electronic and quasiparticle energy levels and to evaluate the electron-hole coupling as a function of the underlying structure. We show that while the presence of defects alters the atomic structure and largely modifies the wave-function nature, leading to defect-localized states at the quasiparticle gap region, the optical excitations remain largely unchanged due to the substantial hybridization of defect and nondefect electron-hole transitions. Our findings suggest that defect-induced surface oxidation supports improved electron transport, both through bound and tunable electronic states and via a mixed nature of the optical transitions, expected to reduce electron-hole defect trapping.

I. INTRODUCTION

Metal oxide semiconductors serve as promising photoanodes for solar-driven water splitting processes [1]. Bismuth vanadate (BiVO$_4$) is a famous example of exceeding interest, being relatively stable, nontoxic, and long lasting, with absorption well within the solar spectrum [2–10], and with suitable electronic properties for efficient oxygen evolution reaction (OER) [4,6,11,12]. Despite these appealing properties, electron conductivity and carrier transport through BiVO$_4$ surfaces are found to be relatively low [13–15], greatly limiting its use in practical applications. This low conductance is typically attributed to fast charge recombination and polaronic interactions [16,17], strongly coupled to the surface structure [18–25] and the conditions in which it was prepared [9,19,26,27]. A broadly explored pathway to improve BiVO$_4$ functionality is through electronic doping upon element substitution and the introduction of vacancies near the interacting BiVO$_4$ surface [16,18,28,29]. These induce modified electronic densities and allow controllable electron mobility and electron-hole recombination rates [14,30–32].

Oxygen vacancies are abundant intrinsic defects in BiVO$_4$ that can also be generated and controlled via external treatments, such as hydrogen annealing and nitrogen flow [16,33,34]. By acting as *n*-type donors, these defects hold the promise to significantly increase the water oxidation reaction yield [15,27,35–37]. From an electronic structure point of view, oxygen vacancies introduce localized electronic states, allowing tunable electronic band gaps and suggesting an enhancement of the separation between photogenerated electrons and holes and an improved absorption cross section of the visible light [15,16,35,38]. On the other hand, localized defect states are considered as active electron-hole recombination centers, which can trap the photogenerated energy carriers—namely, excitons—and consequently reduce the electronic conductivity and the electron and energy transfer efficiency associated with it [27,39–42]. The role of oxygen vacancies in photogenerated carrier transport thus remains controversial, and a comprehensive understanding of the involved defect-induced phototransport mechanisms is still lacking.

Recent density functional theory (DFT) studies found that a structurally stable split oxygen vacancy, in which the vacancy is shared between two neighboring vanadium atoms in the form of a V-O-V bridge, is pivotal to the catalytic reaction that produces molecular oxygen upon water adsorption at thermodynamically stable (001) BiVO$_4$ surfaces [25,35]. These studies showed that the change in surface structure and the underlying chemical bonding due to oxygen vacancies strongly influence the adsorbate. In particular, the main steps within the OER involve either a peroxo bridge between the Bi and V atoms at the surface, or a surface-oxo group evolving into an OOH group [25]. The electronic structure associated with the defects is thus expected to vary due to significant surface-structure modifications within the various steps in the catalytic reaction. The electronic states and the electron-hole binding associated with the vacancies within the catalytic reaction are hence nontrivial, and a predictive assessment of the electronic and excitonic
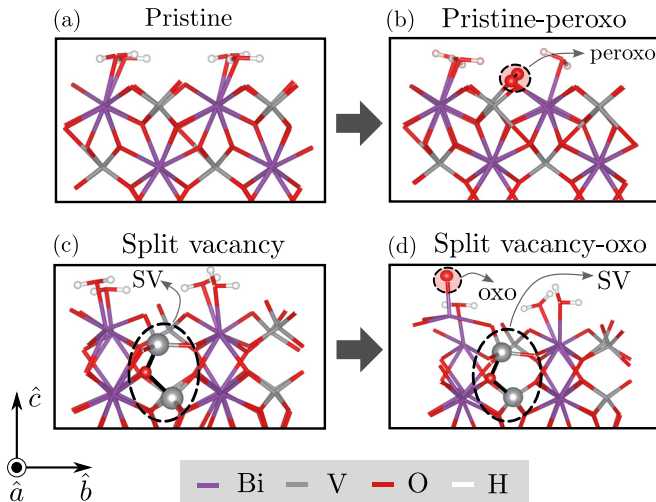
FIG. 1. Four BiVO$_4$ surface structures upon water adsorption, studied in this work: (a) a pristine surface, with full water coverage; (b) a pristine-peroxo surface, in which one water molecule per repeating cell went through oxidation; (c) a surface including a split vacancy with full water coverage; and (d) a split-vacancy-oxo surface, in which one water molecule per repeating cell went through oxidation. Oxidized water molecules are marked by red circles; black arrows represent the structural change upon oxidation. The split vacancy, appearing as a V-O-V bridge, is marked with a black dashed circle and denoted by "SV." Each structure represents the repeating unit cells in the $\hat{a}$, $\hat{b}$ direction; the $\hat{c}$ direction contains six layers as well as additional vacuum, and is shown in the SM [43] for the case of the pristine system.

fine structure as a function of these structural modifications is required.

In this work, we study the effect of oxygen vacancies on the electronic and excitonic properties in BiVO$_4$ upon surface water oxidation. We use DFT and many-body perturbation theory within the *GW* and *GW*-Bethe-Salpeter equation (*GW*-BSE) approximation to calculate the quasiparticle energies and the electron-hole coupling for representative structures found to be stable during the water oxidation stage in the catalytic cycle. We explore how the introduction of oxygen vacancies and the charge localization associated with it influence these properties. Our results show defect-localized states near the valence region, resulting from the underlying chemical bonding, with the quasiparticle band gap largely unchanged upon the inclusion of surface defects. This leads to largely mixed exciton states, hybridizing transitions between defect and nondefect bands. We find that due to this mixing, and unexpectedly, the presence of defects does not alter the exciton binding energy in the examined systems.

II. METHODOLOGY

The studied systems are shown in Fig. 1. Our focus is on the monoclinic scheelite of BiVO$_4$, considered to be the active phase at room temperature. We examine the thermodynamically most stable surface, that is the (001) facet. The calculated unit cell includes six layers, each containing four Bi and four V atoms, with a vacuum of 14 Å separating repeating cells along the $\hat{c}$ direction [see Supplemental Material (SM) [43]].

Atomic structures were relaxed using the Perdew-Burke-Ernzerhof functional revised for solids (PBEsol) following previous studies [35]. This sets a reliable DFT starting point for many-body perturbation theory. We note, however, that polaronic effects may induce additional localization and vary the electronic picture [27]. We consider four main structures occurring within two oxidation pathways, recently suggested to play a key role in the photocatalytic cycle [25]: a pristine BiVO$_4$ surface [Fig. 1(a)]; the same system after one water molecule per cell went through oxidation, resulting in a surface-peroxo group [Fig. 1(b)]; a BiVO$_4$ surface with a subsurface split vacancy (SV) [Fig. 1(c)]; and the same system after one water molecule per cell went through oxidation in the presence of a vacancy, resulting in a surface-oxo group [Fig. 1(d)].

In the following, we present the calculated quasiparticle and excitonic properties associated with these structures, and examine the electronic distribution and electron-hole coupling as a function of oxidation with and without the subsurface defects. To compute the single-particle electronic structure and the wave functions of the examined surfaces, we employ density functional theory (DFT) within the Perdew-Burke-Ernzerhof (PBE) approximation [44] for the exchange-correlation functional including spin-orbit coupling, using the QUANTUM ESPRESSO package [45]. The resulting DFT energies and wave functions are then used as a starting point for our many-body perturbation theory calculations, performed within the BERKELEY*GW* package [46]. We compute quasiparticle energy corrections applying the G_0W_0 approach within the generalized plasmon-pole model for the frequency dependence of the dielectric screening [47]. Following standard converging procedures, we consider a 30 Ry screening cutoff energy and a total of 3500 electronic bands, among them 1280 being occupied. Owing to small band dispersion (see SM) and the large size of the repeating cell, we sample the reciprocal space with a relatively coarse uniform **k**-point grid of $2 \times 2 \times 1$. To account for electron-hole coupling and excitonic properties, we employ the Bethe-Salpeter equation (BSE) formalism within the Tamm-Dancoff approximation [48], while considering 14 valence (occupied) bands and 16 conduction (empty) bands in the coupling matrices (see full computational details in the SM [43]).

III. RESULTS AND DISCUSSION

Figure 2 shows the computed DFT electronic energies and the *GW* quasiparticle energies, as well as the associated band gaps, for the pristine, pristine-peroxo, split-vacancy, and split-vacancy-oxo surface structures, respectively. Due to the relatively small band dispersion in the examined systems (see SM), we present the calculate values only at the Γ point aligned to the highest occupied state that does not have a defect character (absolute alignment between *GW* and DFT of the defect/oxo states is given in the SM [43], as well as full DFT band structures). Blue and orange colors represent the valence band maximum (VBM) and conduction band minimum (CBM), respectively. Black lines represent defect- and surface-oxidized states at the gap region. For the pristine system [Fig. 2(a)], the *GW* opens up the DFT (PBE) gap significantly (by 1.7 eV), to a value of 3.8 eV. This *GW*
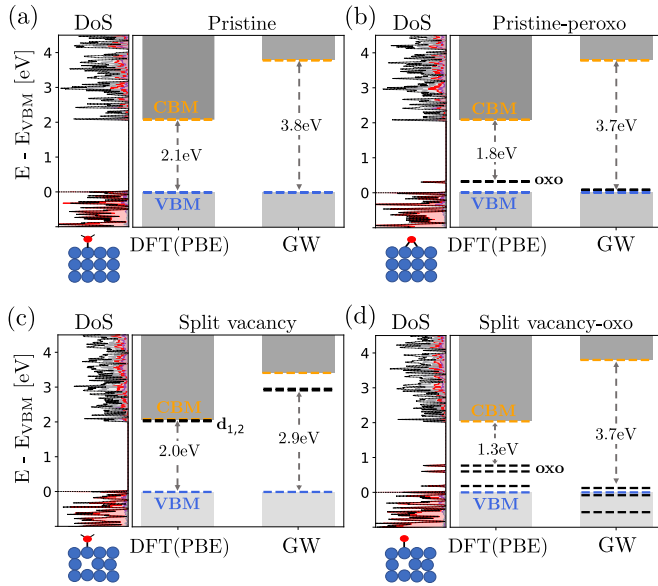
FIG. 2. Calculated DFT and *GW* electron and quasiparticle energies and band gaps, for the (a) pristine, (b) pristine-peroxo, (c) split-vacancy, and (d) split-vacancy-oxo systems at the Γ point. Pristinelike CBM and VBM states are indicated in orange and blue dashed lines, respectively, and additional oxo and defect energy levels are shown as black dashed lines. The projected density of states of each of the surface structures onto the atomic contributions is also shown (violet: Bi; gray: V; red: O; white: H), with the dashed line corresponding to the total density of states.

FIG. 3. (a) Calculated coupling matrix elements $S_{AB} = |\langle \phi_A | \phi_B \rangle|^2$ between DFT electronic states of the pristine and pristine-peroxo systems, where 0 denotes no overlap and 1 denotes complete overlap. (b) Same as in (a) for the comparison between split-vacancy and split-vacancy-oxo systems.

gap is slightly larger than the ones reported before for the bulk system, of 3.4–3.6 eV [8]. The gap increase is expected due to the reduced dielectric screening upon the inclusion of vacuum above the surface [49]. Upon water oxidation and the formation of a surface-peroxo group [Fig. 2(b)], the DFT results show an additional occupied in-gap state, which is shifted down to the VBM when including GW quasiparticle corrections.

In the presence of split vacancies [Fig. 2(c)], defect states marked as $d_{1,2}$ appear in the gap region. In this structure, the *GW* gap of 2.9 eV is significantly smaller than in the pristine case. We associate this gap reduction to fractional occupation at the CBM region, in particular to electrons localized at two V^{4+} sites, previously shown to be responsible for the instability of this structure [25,27,35]. Notably, upon oxidation of the defect surface [Fig. 2(d)], three occupied in-gap states, largely localized on the oxo group, appear at the valence edge region. The quasiparticle *GW* gap obtained is similar to the pristine and pristine-peroxo cases. These results suggest that the presence of oxygen vacancies induces localized states in addition to the pristinelike ones, in agreement with previous findings [15,27,50,51], which change their nature upon surface water oxidation. As we show in the following, these changes in the quasiparticle spectra result from the involved modifications in the chemical bonding around the missing atoms.

To further quantify the defect- and oxidation-induced change in the electronic structure, we examine the wave-function coupling before and after water oxidation, for the two pristine and two split-vacancy structures. For this, we evaluate the coupling matrix elements between the computed
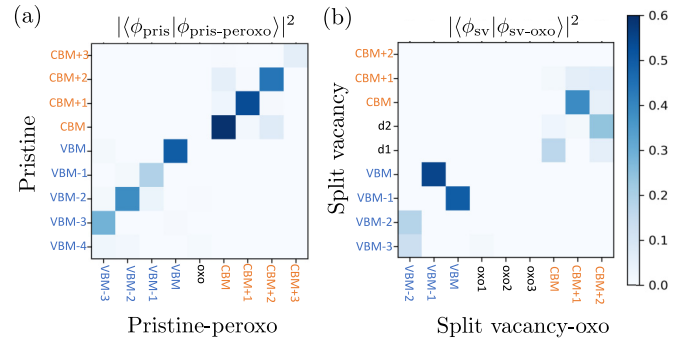
DFT wave functions of each two structures. We define the overlap matrix $S_{AB} = |\langle \phi_A | \phi_B \rangle|^2$, where A and B are different systems, and ϕ is an electronic Kohn-Sham state in a plane-wave basis set. As anticipated above, it is enough to only discuss the S matrix at the Γ point, as the other k points show a similar behavior due to the small band dispersion in the Brillouin zone (see SM [43]). Figure 3(a) shows the computed overlap between the pristine and pristine-peroxo structures, $S = |\langle \phi_{\text{pris}} | \phi_{\text{pris-peroxo}} \rangle|^2$. For this case, we find substantial coupling between the two systems—before and after surface oxidation—at the valence and conduction areas. As expected, the additional peroxo-localized in-gap states have negligible overlap with any of the pristine bands, suggesting that the local modification due to the surface oxidation and the peroxo formation is small.

In contrast, in the presence of subsurface split-vacancy defects, this picture becomes more complicated. The computed overlap between the split-vacancy and split-vacancy-oxo structures, $S = |\langle \phi_{\text{sv}} | \phi_{\text{sv-oxo}} \rangle|^2$ [Fig. 3(b)] shows that while few bands around the valence and conduction area remain of a similar nature, the defect states largely change their nature after surface oxidation. As a result, we find negligible overlap between defect states with water surface adsorbates [Fig. 2(c)] and defect states with oxidized adsorbates [Fig. 2(d)]. In other words, there are significant changes in the wave-function nature due to the surface-oxo bonding and the structural changes associated with it. We further note that the overlap matrix elements vanish almost completely when comparing between the pristine and the split-vacancy structures, and between the pristine-peroxo and the split-vacancy-oxo structures (see SM [43]). This suggests that the presence of oxygen vacancies leads to changes in the underlying bonding, which completely modifies the electronic wave functions. In addition, surface oxidation changes the surface bonding in the presence of defects, leading to the observed modifications in the electronic and quasiparticle spectra.

Having identified the change in electronic states and quasiparticle energy levels upon surface water oxidation and in the presence of defects, we now turn to compute the electron-hole coupling and the associated optical and excitonic properties. Figure 4 shows the calculated *GW*-BSE absorption spectra
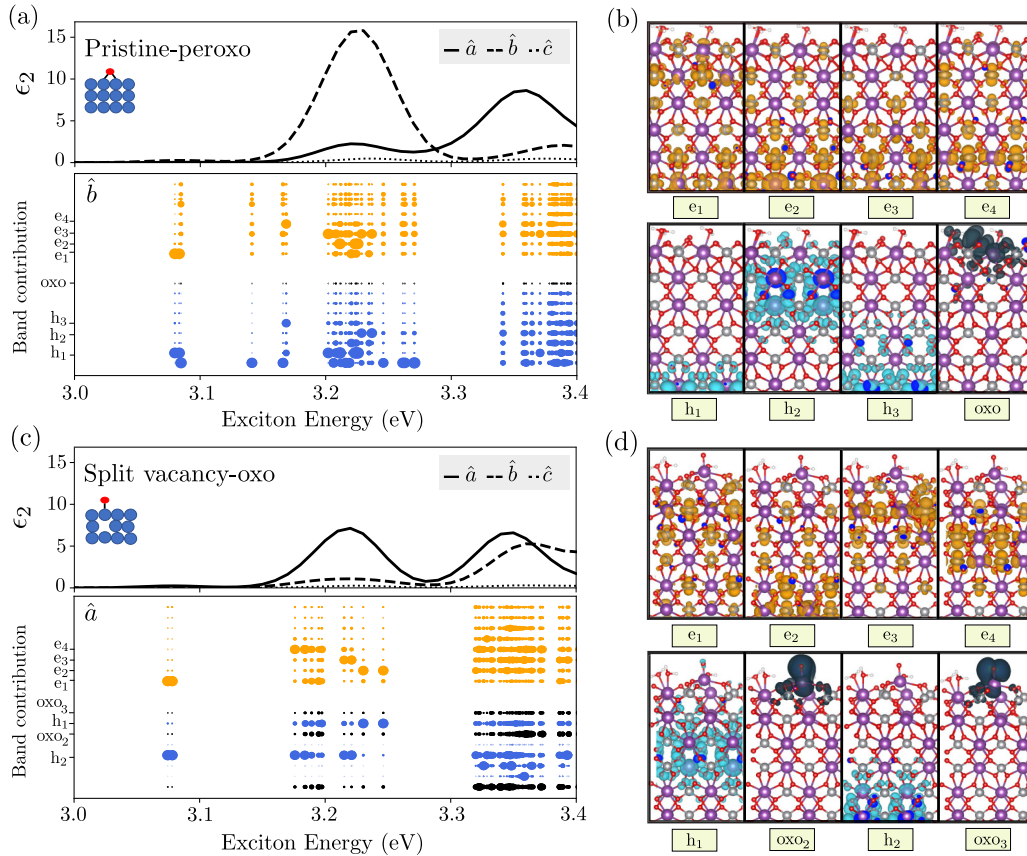
FIG. 4. (a) Calculated *GW*-BSE absorption spectra for the three main polarization directions, as well as electron-hole transitions contributing to the absorption peaks, for the pristine-peroxo system. Contributions from occupied (hole) bands are shown in blue, from unoccupied (electron) bands in orange, and from localized peroxo and oxo bands in black. Each dot in the lower panel represents the band contribution to the exciton as a function of the excitation energy, weighted by the oscillator strength at the dominating polarization direction ($\hat{b}$). (b) Representative wave-function distributions corresponding to the electron and hole Kohn-Sham states with the largest contribution to the low-energy absorption peaks. (c), (d) Same as in (a), (b) for the split-vacancy-oxo system. The exciton contributions are weighted with oscillator strength at the $\hat{a}$ polarization direction, which is the dominating one in this structure.

of the two oxidized surfaces with and without subsurface defects, pristine-peroxo and split-vacancy-oxo, upon optical excitation with light polarized at the three main crystal directions. The absorption peaks are further analyzed through the electron-hole transitions composing them. We first note that in both structures, the absorption oscillator strengths at the $\hat{a}$ and $\hat{b}$ polarization directions are much larger than at the $\hat{c}$ direction, suggesting that in-plane excitations dominate the spectra. However, while the lowest excitation peak in the pristine-peroxo case is at the $\hat{b}$ polarization direction, in the split-vacancy-oxo case it is at the $\hat{a}$ direction, serving as another signature of the significant underlying structural changes involved upon the presence of defects.

For the pristine-peroxo structure [Fig. 4(a)], the lowest bright excitation is at 3.08 eV, and the low-energy absorption peak is at 3.23 eV. These excitation energies are in good agreement with experimental findings, where the optical gap is found at ~3 eV [22,52–54]. The differences between the computed quasiparticle and optical gaps point to a relatively large exciton binding energy, on the order of 0.6 eV, suggesting strong electron-hole coupling. We note that this energy difference does not include lattice relaxation processes, which can largely reduce the band gap in these materials [11,52,53,55].

The computed excitation energies for the nonoxidized pristine case are very similar (see the computed absorption in the SM [43]), and are in good agreement with previous calculations for the bulk pristine system [8]. Such an agreement between surface and bulk structures can be explained by the local nature of the electron-hole interactions, leading to small long-range surface effects on the computed excitation energies. This points to larger exciton binding energies at the surface compared to the bulk, as expected, due to an increase in the quasiparticle gap while the optical gap remains similar.

The exciton coefficients for each excitonic state S, $A_{vc\mathbf{k}}^{S}$, quantify the coupling between an electron at band c and a hole at band v, at the k point $\mathbf{k}$. Electron-hole transitions composing the absorption spectra of the pristine-peroxo system are shown below the corresponding absorption energies in Fig. 4(a). The dot size represents the relative magnitude of the normalized exciton contribution, $\sum_{v\mathbf{k}} |A_{vc\mathbf{k}}^{S}|^2$ for unoccupied (c) bands and $\sum_{c\mathbf{k}} |A_{vc\mathbf{k}}^{S}|^2$ for occupied (v) bands, summed over all k points and scaled with the oscillator strength at the dominating polarization direction, so that only bright peaks are shown (contributions weighted by the other polarization directions are shown in the SM [43]). This analysis allows us to quantify the contribution from each electron/hole state

(orange/blue dots, respectively) to each one of the computed excitons. Black dots represent localized and occupied surface oxidation states, associated with the dashed black energy levels in Fig. 2(b). The electron/hole wave functions with the most significant contributions to low-lying excitons are shown in Fig. 4(b). Notably, the lowest bright exciton around 3.1 eV is primarily composed of transitions between the conduction electron band e_1 and a hole band below the valence region h_1. We note that this hole state is mainly localized at the bottom layer and thus may have increased delocalization when more layers are included, bringing it closer to the higher-energy hole states at the valence region. The peak around 3.2 eV already includes multiple electron-hole transitions, with additional contributions from occupied states localized at the oxidized surface-peroxo group, as well as other hole and electron states which are not associated with the surface-peroxo group.

This hybridized excitation nature is also present upon the inclusion of subsurface defects in the oxidized structure [Figs. 4(c) and 4(d)]. The lowest bright excitation is at 3.08 eV, and the low-energy absorption peak is at 3.22 eV, similarly to the pristine case. In contrast to the nondefective structure, in this case, defect-localized oxo states play a significant role in the excitation. The electron-hole contributions from defect-induced oxo states are shown as black dots in Fig. 4(c) and the associated wave functions are presented in Fig. 4(d). Notably, our *GW*-BSE results suggest that the associated excitons strongly mix defect and nondefect transitions. As a result, the overall peak position does not change compared to the nondefect case. Since the quasiparticle gap is also similar in both systems, the exciton binding energy associated with the low-energy excitation peak remains unchanged upon defect formation. However, the absorption contribution at the various polarization directions changes due to the modification in the underlying structure, reflecting a change in the directionality of the wave-function components, as discussed above.

Our results show that the low-energy exciton peaks, dominating the photoexcitation, are of a highly hybridized nature, which eventually leads to comparable excitation energies between the nondefect and the defect oxidized surface structures. This is a direct outcome of the localized nature of both nondefect and defect states in this system, as is also evident by the large quasiparticle gap and the electron-hole binding energies found with and without defects. This suggests that the role of oxygen vacancies in the associated catalytic cycle mainly comes to play in the structural modification and stabilization upon water oxidation. Such a modification leads to near-gap surface states which can support the improved charge transfer, in particular upon defect charging expected to occur through electronic transport and pushing those bands deeper into the gap [15]. However, our computations show that the electron-hole transitions composing the excitons are hybridized and include both pristine and defect states, suggesting that defects cannot be trivially treated as charge traps. This implies that the many-body excitonic picture associated with photogeneration processes on BiVO$_4$ surfaces in the presence of defects can support improved carrier transport.

IV. CONCLUSION

To conclude, in this work we explored how subsurface defects alter the electronic and excitonic properties in BiVO$_4$ upon surface water oxidation. We find that the state localization due to structural modifications strongly influences the quasiparticle charge distributions and energy levels. However, oxygen vacancies only slightly change the exciton states, due to hybridized electron-hole transitions which mix defect and pristine states at similar energy regions. Our study presents a connection between the change in chemical bonding due to the presence of defects and the subsequent variations in the electronic band structure, wave functions, and optical excitations, demonstrating the nontrivial effect of defects on the mechanisms in which light is stored and energy is transferred in BiVO$_4$.

[1] C. Jiang, S. J. Moniz, A. Wang, T. Zhang, and J. Tang, Chem. Soc. Rev. **46**, 4645 (2017).

[2] Q. Jia, K. Iwashina, and A. Kudo, Proc. Natl. Acad. Sci. USA **109**, 11564 (2012).

[3] A. Kudo, K. Ueda, H. Kato, and I. Mikami, Catal. Lett. **53**, 229 (1998).

[4] I. D. Sharp, J. K. Cooper, F. M. Toma, and R. Buonsanti, ACS Energy Lett. **2**, 139 (2017).

[5] H. L. Tan, R. Amal, and Y. H. Ng, J. Mater. Chem. A **5**, 16498 (2017).

[6] K. R. Tolod, S. Hernández, and N. Russo, Catalysts **7**, 13 (2017).

[7] Z. Zhao, Z. Li, and Z. Zou, Phys. Chem. Chem. Phys. **13**, 4746 (2011).

[8] J. Wiktor, I. Reshetnyak, F. Ambrosio, and A. Pasquarello, Phys. Rev. Materials **1**, 022401(R) (2017).

[9] T. Das, X. Rocquefelte, R. Laskowski, L. Lajaunie, S. Jobic, P. Blaha, and K. Schwarz, Chem. Mater. **29**, 3380 (2017).

[10] Y. Wang, H. Shi, S. Ge, L. Zhang, X. Wang, and J. Yu, Sens. Actuators, B **336**, 129746 (2021).

[11] J. K. Cooper, S. Gul, F. M. Toma, L. Chen, P.-A. Glans, J. Guo, J. W. Ager, J. Yano, and I. D. Sharp, Chem. Mater. **26**, 5365 (2014).

[12] Y. Park, K. J. McDonald, and K.-S. Choi, Chem. Soc. Rev. **42**, 2321 (2013).

[13] F. F. Abdi, T. J. Savenije, M. M. May, B. Dam, and R. van de Krol, J. Phys. Chem. Lett. **4**, 2752 (2013).

[14] A. J. Rettie, H. C. Lee, L. G. Marshall, J.-F. Lin, C. Capan, J. Lindemuth, J. S. McCloy, J. Zhou, A. J. Bard, and C. B. Mullins, J. Am. Chem. Soc. **135**, 11389 (2013).

[15] H. Seo, Y. Ping, and G. Galli, Chem. Mater. **30**, 7793 (2018).

[16] T. W. Kim, Y. Ping, G. A. Galli, and K.-S. Choi, Nat. Commun. **6**, 8769 (2015).

[17] H. S. Park, K. E. Kweon, H. Ye, E. Paek, G. S. Hwang, and A. J. Bard, J. Phys. Chem. C **115**, 17870 (2011).

[18] S. Wang, P. Chen, Y. Bai, J.-H. Yun, G. Liu, and L. Wang, Adv. Mater. **30**, 1800486 (2018).

[19] S. Hammes-Schiffer and G. Galli, Nat. Energy **6**, 700 (2021).

[20] J. Hu, W. Chen, X. Zhao, H. Su, and Z. Chen, ACS Appl. Mater. Interfaces **10**, 5475 (2018).

[21] D. Li, Y. Liu, W. Shi, C. Shao, S. Wang, C. Ding, T. Liu, F. Fan, J. Shi, and C. Li, ACS Energy Lett. **4**, 825 (2019).

[22] H. Wu, R. Irani, K. Zhang, L. Jing, H. Dai, H. Y. Chung, F. F. Abdi, and Y. H. Ng, ACS Energy Lett. **6**, 3400 (2021).

[23] S. Lardhi, L. Cavallo, and M. Harb, J. Phys. Chem. Lett. **11**, 5497 (2020).

[24] A. Kahraman, M. B. Vishlaghi, I. Baylam, H. Ogasawara, A. Sennaroglu, and S. Kaya, J. Phys. Chem. Lett. **11**, 8758 (2020).

[25] P. Nikačević, F. S. Hegner, J. R. Galán-Mascarós, and N. López, ACS Catal. **11**, 13416 (2021).

[26] G.-L. Li, RSC Adv. **7**, 9130 (2017).

[27] W. Wang, P. J. Strohbeen, D. Lee, C. Zhou, J. K. Kawasaki, K.-S. Choi, M. Liu, and G. Galli, Chem. Mater. **32**, 2899 (2020).

[28] D. Li, W. Wang, D. Jiang, Y. Zheng, and X. Li, RSC Adv. **5**, 14374 (2015).

[29] R. Fernández-Climent, S. Giménez, and M. García-Tecedor, Sustainable Energy Fuels **4**, 5916 (2020).

[30] W. Luo, Z. Yang, Z. Li, J. Zhang, J. Liu, Z. Zhao, Z. Wang, S. Yan, T. Yu, and Z. Zou, Energy Environ. Sci. **4**, 4046 (2011).

[31] F. F. Abdi, L. Han, A. H. Smets, M. Zeman, B. Dam, and R. Van De Krol, Nat. Commun. **4**, 2195 (2013).

[32] Y. Liang, T. Tsubota, L. P. Mooij, and R. van de Krol, J. Phys. Chem. C **115**, 17594 (2011).

[33] J. K. Cooper, S. B. Scott, Y. Ling, J. Yang, S. Hao, Y. Li, F. M. Toma, M. Stutzmann, K. Lakshmi, and I. D. Sharp, Chem. Mater. **28**, 5761 (2016).

[34] N. Daelman, F. S. Hegner, M. Rellán-Piñeiro, M. Capdevila-Cortada, R. García-Muelas, and N. López, J. Chem. Phys. **152**, 050901 (2020).

[35] F. S. Hegner, D. Forrer, J. R. Galan-Mascaros, N. López, and A. Selloni, J. Phys. Chem. Lett. **10**, 6672 (2019).

[36] A. C. Ulpe, B. Anke, S. Berendts, M. Lerch, and T. Bredow, Solid State Sci. **75**, 39 (2018).

[37] J. Hu, H. He, X. Zhou, Z. Li, Q. Shen, W. Luo, A. Alsaedi, T. Hayat, Y. Zhou, and Z. Zou, Chem. Commun. **55**, 5635 (2019).

[38] W.-J. Yin, S.-H. Wei, M. M. Al-Jassim, J. Turner, and Y. Yan, Phys. Rev. B **83**, 155102 (2011).

[39] X. Zhao, J. Hu, X. Yao, S. Chen, and Z. Chen, ACS Appl. Energy Mater. **1**, 3410 (2018).

[40] T.-Y. Yang, H.-Y. Kang, U. Sim, Y.-J. Lee, J.-H. Lee, B. Koo, K. T. Nam, and Y.-C. Joo, Phys. Chem. Chem. Phys. **15**, 2117 (2013).

[41] T. Liu, M. Cui, and M. Dupuis, J. Phys. Chem. C **124**, 23038 (2020).

[42] S. Selim, E. Pastor, M. García-Tecedor, M. R. Morris, L. Francàs, M. Sachs, B. Moss, S. Corby, C. A. Mesa, S. Gimenez, A. Kafizas, A. A. Bakulin, and J. R. Durrant, J. Am. Chem. Soc. **141**, 18791 (2019).

[43] See Supplemental Material at http://link.aps.org/supplemental/10.1103/PhysRevMaterials.6.065402 for computational details (section I), band structures of the examined systems (section II), absolute defect state alignment analysis (section III), additional details of the computed overlap matrix (section IV), theoretical basis for the band contributions to the excitonic peaks (section V) and additional absorption data (section VI).

[44] J. P. Perdew, K. Burke, and M. Ernzerhof, Phys. Rev. Lett. **77**, 3865 (1996).

[45] P. Giannozzi, S. Baroni, N. Bonini, M. Calandra, R. Car, C. Cavazzoni, D. Ceresoli, G. L. Chiarotti, M. Cococcioni, I. Dabo *et al.*, J. Phys.: Condens. Matter **21**, 395502 (2009).

[46] J. Deslippe, G. Samsonidze, D. A. Strubbe, M. Jain, M. L. Cohen, and S. G. Louie, Comput. Phys. Commun. **183**, 1269 (2012).

[47] M. S. Hybertsen and S. G. Louie, Phys. Rev. B **34**, 5390 (1986).

[48] M. Rohlfing and S. G. Louie, Phys. Rev. Lett. **81**, 2312 (1998). Phys. Rev. B. **62**, 4927 (2000).

[49] D. Y. Qiu, F. H. da Jornada, and S. G. Louie, Phys. Rev. B **93**, 235435 (2016).

[50] N. Österbacka and J. Wiktor, J. Phys. Chem. C **125**, 1200 (2021).

[51] N. Österbacka, F. Ambrosio, and J. Wiktor, J. Phys. Chem. C **126**, 2960 (2022).

[52] S. Stoughton, M. Showak, Q. Mao, P. Koirala, D. A. Hillsberry, S. Sallis, L. F. Kourkoutis, K. Nguyen, L. F. J. Piper, D. A. Tenne, N. J. Podraza, D. A. Muller, C. Adamo, and D. G. Schlom, APL Mater. **1**, 042112 (2013).

[53] J. K. Cooper, S. Gul, F. M. Toma, L. Chen, Y.-S. Liu, J. Guo, J. W. Ager, J. Yano, and I. D. Sharp, J. Phys. Chem. C **119**, 2969 (2015).

[54] V. F. Kunzelmann, C.-M. Jiang, I. Ihrke, E. Sirotti, T. Rieth, A. Henning, J. Eichhorn, and I. D. Sharp, J. Mater. Chem. A (2022), doi:10.1039/d1ta10732a.

[55] D. Payne, M. Robinson, R. Egdell, A. Walsh, J. McNulty, K. Smith, and L. Piper, Appl. Phys. Lett. **98**, 212110 (2011).